LETTER

Tuning the Solvation Structure in Aqueous Zinc Batteries to Maximize Zn-Ion Intercalation and Optimize Dendrite-Free Zinc Plating

Chang Li, Ryan Kingsbury, Laidong Zhou, Abhinandan Shyamsunder, Kristin A. Persson, and Linda F. Nazar*

Read Online

ACCESS | Metrics & More | Article Recommendations | SI Supporting Information

ABSTRACT: Aqueous zinc batteries are recognized to suffer from H^+/Zn^{2+} coinsertion in the cathode, but few approaches have been reported to suppress deleterious H^+ intercalation. Herein, we realize this goal by tuning the solvation structure, using $LiV_2(PO_4)_3$ (LVP) as a model cathode. Phase conversion of LVP induced by H^+ intercalation is observed in 4 m $Zn(OTf)_2$, whereas dominant Zn^{2+} insertion is confirmed in a $ZnCl_2$ water-in-salt electrolyte (WiSE). This disparity is ascribed to the complete absence of free water and a strong $Zn^{2+}-H_2O$ interaction in the latter that interrupts the H_2O hydrogen bonding network, thus suppressing H^+ intercalation. On the basis of this strategy, a novel PEG-based hybrid electrolyte is designed to replace the corrosive $ZnCl_2$ WiSE. This system exhibits an optimized Zn^{2+} solvation sheath with a similar low free water content, showing not only much better suppression of H^+ intercalation but also highly reversible Zn plating/stripping with a CE of ∼99.7% over 150 cycles.
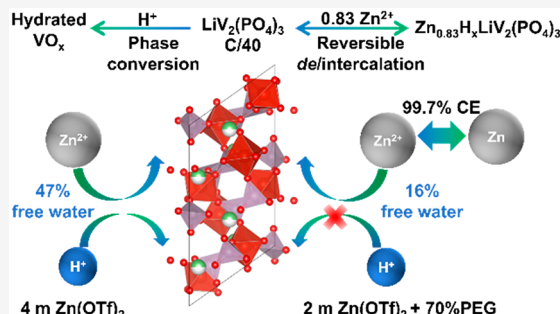
Owing to the high electrodeposition potential of Zn^{2+} (∼−0.76 V vs SHE), the high theoretical volumetric capacity of the Zn anode (5850 mAh mL^{-1}) and the advantages of low-cost, high-safety, and eco-friendly operation, aqueous zinc metal batteries (AZMBs) are becoming one of the most attractive technologies for large-scale stationary energy storage.[1−3] Much work has focused on developing cathode materials for AZMBs, including MnO_2,[4] $Zn_{0.25}V_2O_5$·nH_2O,[5] and many others. However, recent studies have found that the high electrochemical capacity of these metal oxides is not solely due to Zn^{2+} insertion/extraction but also relies on H^+ (de)intercalation.[6−11] Proton intercalation results in the formation of layered double-hydroxide salts (LDH, for example, $Zn_4SO_4(OH)_6$·$5H_2O$) on the surface of metal oxides,[8−10] which aids the reversible and stable operation of metal oxides due to its unique buffering mechanism.[8] On the other hand, the LDH forms an insulating layer on the oxide surface that detaches from the electrode over time, leading to loss of active material. Proton intercalation has now been generally accepted as a common phenomenon for metal oxides in AZMBs.

Studies involving polyanion compounds similarly showed that either H^+ (or Na^+) insertion occurs along with Zn^{2+}

intercalation.[12−14] For example, by analyzing the differential capacity curves (dQ/dV) of layered $VOPO_4$·xH_2O cathode in different electrolytes, Sun et al. found that H^+ intercalation played a dominant role in an electrolyte comprised of 5 m $ZnCl_2$/0.8 m H_3PO_4.[13] Not surprisingly, on increasing the concentration of $ZnCl_2$ to 10−13 m, Zn^{2+} was suggested to dominate the intercalation process based on the higher peak intensity of the Zn contribution in the dQ/dV curve. The factors responsible for Zn^{2+} versus H^+ intercalation (aside from concentration) were not investigated in this study. Monoclinic $LiV_2(PO_4)_3$ was reported to be a superior host for AZMBs and can be cycled at an exceptionally high rate of 60 C.[15] As the high charge density of Zn^{2+} would likely result in limits to solid-state diffusion at this current density and significant structural distortion in monoclinic $V_2(PO_4)_3$,[16] a fundamen-
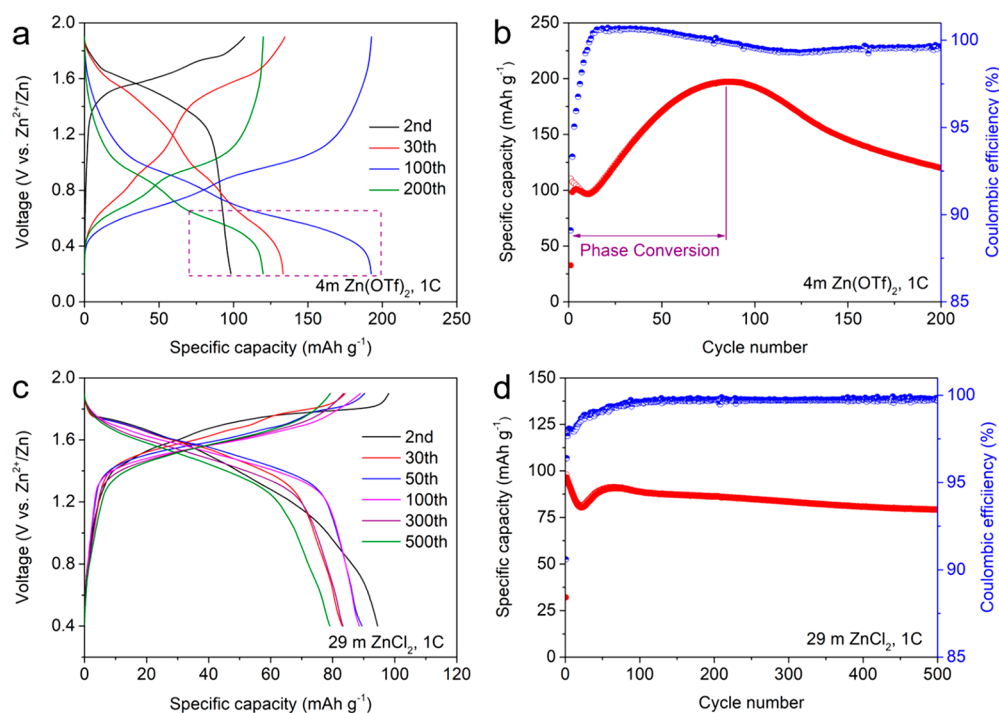
Figure 1. Charge−discharge curves of LVP during different cycles and corresponding capacity retention at 1 C (= 136 mA g^{-1}) in (a, b) 4 m Zn(OTf)$_2$ and (c, d) 29 m ZnCl$_2$ WiSE.

tally different mechanism based on H$^+$ intercalation rather than exclusive Zn^{2+} insertion has been proposed to account for this high-rate performance.[11] Recently, an approach to favor Zn^{2+} intercalation was reported for a VPO$_4$F host lattice based on a hybrid electrolyte (water + propylene carbonate); however, proton intercalation still could not be fully suppressed. A multiphase mixture with overall composition of Zn$_{0.3}$H$_y$VPO$_4$F was formed on discharge, but the implicit existence of a more highly zincated phase could not be quantified.[14]

Herein, we demonstrate that solvation-structure engineering of aqueous Zn electrolytes (AZEs) is an effective method to suppress H$^+$ intercalation and realize dominant Zn^{2+} intercalation. To establish proof-of-concept, we chose LiV$_2$(PO$_4$)$_3$ (LVP) as the cathode platform and compared its electrochemistry in two previously reported electrolytes, 4 m (molality, mol/kg) Zn(OTf)$_2$ and 29 m ZnCl$_2$ "water-in-salt" electrolytes (WiSE), as well as a newly designed hybrid electrolyte developed by incorporating polyethylene glycol 400 (PEG 400) and water as a cosolvent with Zn(OTf)$_2$ as the salt. Importantly, we explore the H-bonding network, free water fraction, Zn^{2+}-solvation structure and their roles in Zn^{2+} vs H$^+$ intercalation in all three electrolyte systems, using experimental and computational methods to understand why the PEG-based hybrid electrolyte exhibits the least H$^+$ intercalation and the most dominant Zn^{2+} intercalation.

The synthesized Li$_3$V$_2$(PO$_4$)$_3$ (Li$_3$VP)−carbon composite consists of approximately 1 μm aggregate crystallites that are enclosed by conductive carbon (Figure S1). The ∼8.75% carbon content was confirmed by thermogravimetric analysis (TGA), as shown in Figure S2. LiV$_2$(PO$_4$)$_3$ (LVP) electrodes were prepared by charging Li$_3$VP electrodes to 1.85 V (vs Zn^{2+}/Zn) in 4 m Zn(OTf)$_2$, where two Li$^+$ per formula unit of Li$_3$VP was successfully extracted. Rietveld refinement of the powder X-ray diffraction (XRD) pattern indicates that all LVP reflections are well indexed to a monoclinic LVP phase with a

space group of $P2_1/c$. A unit cell volume contraction of 7.3% upon two Li$^+$-ion extraction is in close accord with the reported value (Tables S1 and S2).[17]

The electrochemistry of LVP in 4 m Zn(OTf)$_2$ was compared to 29 m ZnCl$_2$ WiSE electrolytes at a 1 C rate (discharge/charge of 1 Zn^{2+} in 1 h). Very different electrochemical behavior was observed. As shown in Figure 1a, in 4 m Zn(OTf)$_2$ a new discharge plateau below 0.5 V accompanies the increase in capacity and becomes more dominant as the cycle number rises, suggesting a phase conversion process (Figure 1b). That process is especially evident in the differential capacity curve (Figure S3a). The new lower-voltage plateau was also identified by Wang et al. for a spray-dried LVP cathode,[15] but its origin was not disclosed. It should be noted that this low-voltage discharge plateau (∼0.5 V vs Zn) is also seen in VO$_x$-based cathode materials, indicating H$^+$ intercalation and the formation of LDHs.[8−10] In contrast, no lower-voltage plateau was observed in ZnCl$_2$ WiSE, only a minor activation-like process (Figures 1c, d and S3b). Strikingly different from the high maximum capacity of 200 mAh g^{-1} exhibited in 4 m Zn(OTf)$_2$, a more realistic discharge capacity of about 90 mAh g^{-1} was recorded at the 60th cycle in ZnCl$_2$ WiSE after the initial activation process. LVP also shows poor cycling stability in 4 m Zn(OTf)$_2$ with only 61% capacity retained after cycling at a rate of 1 C for 200 cycles (Figure 1b), whereas very good cycling stability with a high capacity retention of about 88% in ZnCl$_2$ WiSE was observed at the same rate for 500 cycles (Figure 1d). Such contrasting electrochemistry is also exhibited at higher current densities, as shown in Figure S4.

The abnormal electrochemistry observed in 4 m Zn(OTf)$_2$ can be attributed to the decomposition of LVP and the formation of hydrated vanadium oxides (VO$_x$) phases based on our X-ray diffraction (XRD) studies. The XRD patterns in Figure 2a show that monoclinic LVP gradually disappears in 4
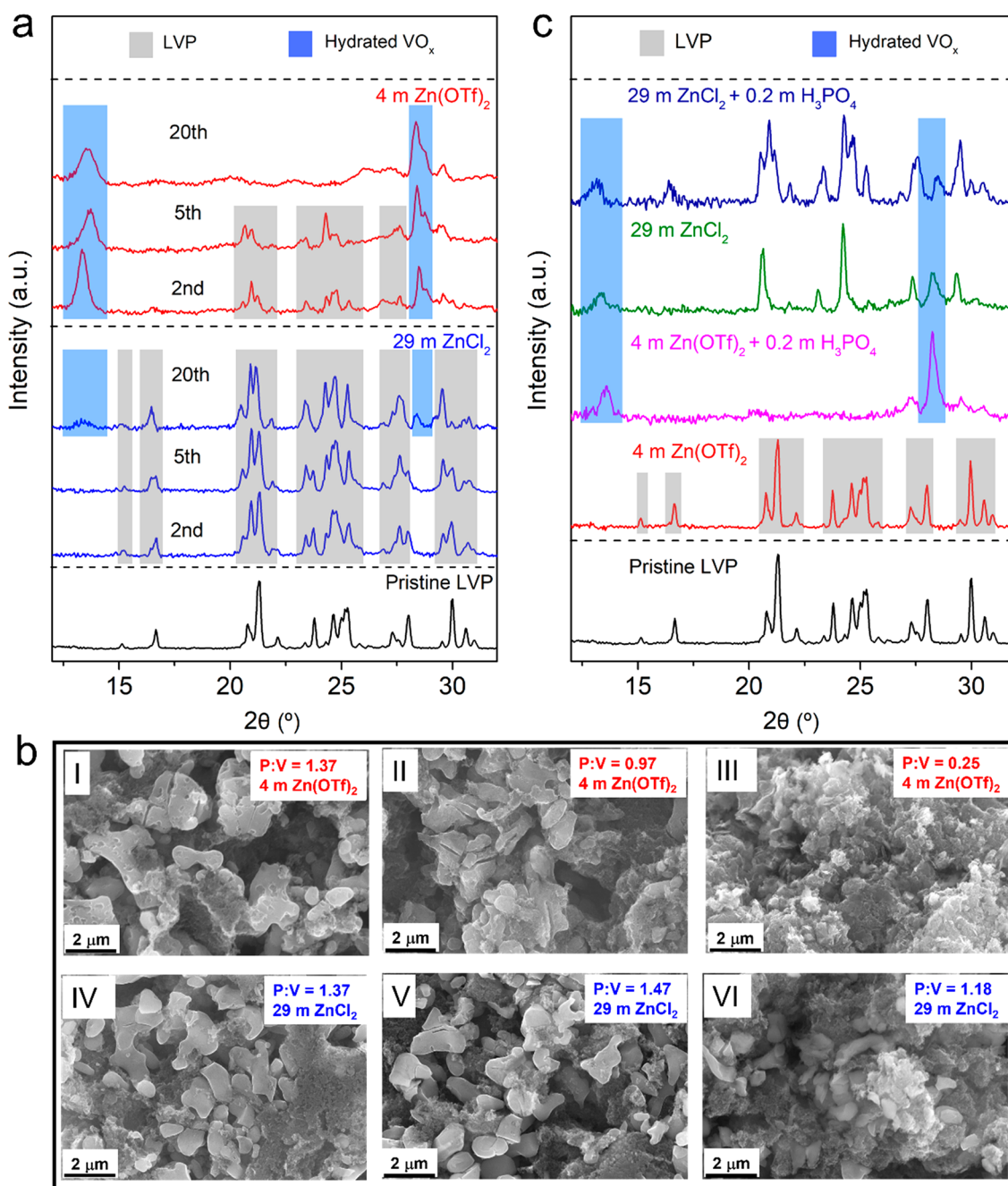
Figure 2. (a) XRD patterns of fully charged LVP electrodes at C/5 after different cycles and (b) corresponding SEM images and P:V ratios collected by EDX at the 2nd (I, IV), 5th (II, V), and 20th (III, VI) cycle. (c) XRD patterns of LVP electrodes soaked in various electrolytes for 24 h.

m $Zn(OTf)_2$ as the cycle number increases. Simultaneously, two new reflections assigned to hydrated VO_x phases appear, and finally become the major components of the active material (Figure S5). The morphology of the LVP electrodes during this phase conversion process was determined by SEM (Figure 2b). The well-crystallized particles gradually decompose and exhibit severe loss of crystallinity on cycling. EDX mapping also reveals a gradually decreasing P:V ratio (Figure S6a), further supporting the formation of hydrated VO_x phases. In contrast, the structure of LVP was better maintained in $ZnCl_2$ WiSE as cycling progressed (Figure 2a), although two small new peaks corresponding to hydrated VO_x appear over a period of 20 cycles. Figures 2b and S6b shows that the

morphology and P:V ratio of LVP electrodes only change slightly in $ZnCl_2$ WiSE, where clear and distinguishable crystalline particles are preserved upon cycling.

To explore whether hydrated VO_x phases result from vanadium dissolution of LVP or H+ uptake, LVP electrodes were soaked in 4 m $Zn(OTf)_2$, $ZnCl_2$ WiSE, and with the addition of 0.2 m H_3PO_4 to both electrolytes. Figure 2c shows the XRD patterns of LVP electrodes that were soaked in the above four electrolytes for 24 h. The intensity and position of the LVP reflections compared to the pristine material remain unchanged in 4 m $Zn(OTf)_2$, indicating insignificant vanadium dissolution. However, a major change in the XRD pattern was observed for the electrode soaked in $ZnCl_2$ WiSE for 24 h,

which we ascribe to ion-exchange of Li^+ for Zn^{2+} owing to a similar ionic radius and the ultrahigh Zn concentration. With the addition of 0.2 m H_3PO_4, this ion exchange process is partially suppressed. While the LVP phase completely disappears in 4 m $Zn(OTf)_2$ + 0.2 m H_3PO_4, two new distinct and characteristic peaks of hydrated VO_x appear. This XRD pattern is almost the same as that of fully charged LVP after 20 cycles at C/5 in 4 m $Zn(OTf)_2$ (Figure S7), suggesting H^+ uptake is responsible for generating these hydrated VO_x phases.

Dominant Zn^{2+} intercalation of LVP in $ZnCl_2$ WiSE was confirmed by Rietveld refinement of the XRD pattern of fully discharged LVP (at a C/40 rate). As shown in Figure 3a and
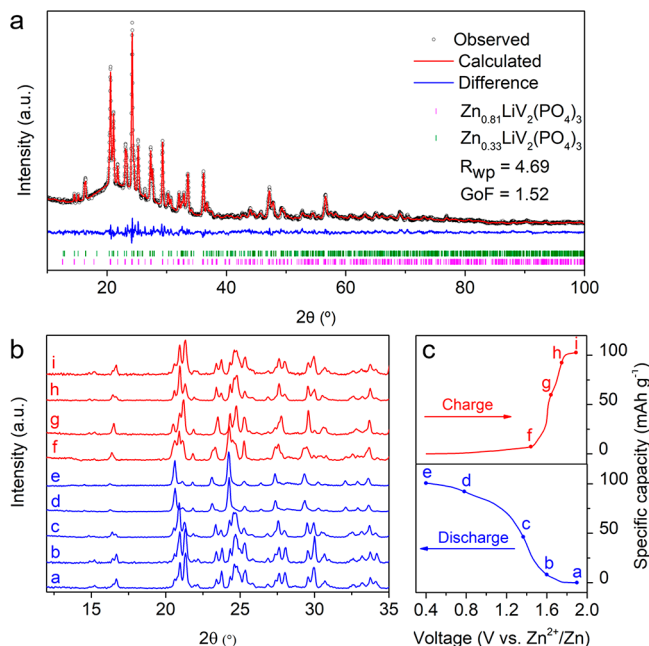

Figure 3. (a) Rietveld fit result of the 2nd fully discharged LVP electrode in 29 m $ZnCl_2$ at C/40. (b) Ex situ XRD patterns of LVP during the 2nd cycle and (c) corresponding charge−discharge curve in 29 m $ZnCl_2$ at C/5.

Table S3, two independent phases with different amounts of intercalated Zn^{2+} coexist: 59 wt % of a Zn-rich phase ($Zn_{0.81}LiV_2(PO_4)_3$) and 41 wt % of a Zn-deficient phase ($Zn_{0.33}LiV_2(PO_4)_3$). The average fraction of inserted Zn^{2+} was 0.61 per formula unit, corresponding to an electrochemical capacity of 83 mAh g^{-1}. While EDX also shows that around 0.60 Zn^{2+} (~81 mAh g^{-1}) has intercalated into the lattice (Figure S8), the actual discharge capacity is 115 mAh g^{-1} (≈0.85 Zn^{2+}, Figure S9). The difference of 34 mAh g^{-1} we ascribe to H^+ cointercalation. Thus, over 70% of the capacity can be attributed to Zn^{2+} intercalation in the LVP lattice. This value is much higher than that reported (<30%) for V_3O_7,[8] $Ca_{0.34}V_2O_5 \cdot 1.16H_2O$,[9] and VPO_4F.[18] The (de)intercalation of Zn^{2+} into LVP was also confirmed by an ex situ XRD study conducted at C/5 on the second cycle (Figure 3b and c). With the increasing fraction of intercalated Zn^{2+}, peaks continuously merge and shift to lower angle. During Zn^{2+} deintercalation, exactly the converse process was observed, with gradual peak separation and shift to higher angles. This demonstrates the good structural reversibility of LVP as a host for Zn^{2+} insertion/extraction.

The electrochemistry observed for LVP in 4 m $Zn(OTf)_2$ can be ascribed to the decomposition of active materials induced by H^+ intercalation, which likely produces hydrated vanadium oxides as discussed above. This H^+ intercalation process can be largely suppressed by using $ZnCl_2$ WiSE, resulting in dominant and reversible Zn^{2+}-(de)intercalation electrochemistry. Suppression of H^+ intercalation is due to an interrupted H_2O hydrogen bonding network and the existence of only a small fraction of free water molecules in $ZnCl_2$−WiSE as we show below via molecular dynamics (MD) simulations. A systematic study on a similar $ZnCl_2$−WiSE has been carried out by Ji et al.[19,20] Their studies, using FTIR spectroscopy, revealed a decreased O−H symmetric stretch (3200 cm^{-1}) and an increased asymmetric stretch (3400 cm^{-1}) on increasing the concentration of $ZnCl_2$ from 5 to 30 m, suggestive of a strong Zn^{2+}-water interaction that triggers interruption of H_2O hydrogen bonding network.[19] Furthermore, their MD simulations show that the number of uncoordinated free water molecules in the electrolyte significantly decreases from 10 m $ZnCl_2$ to 30 m $ZnCl_2$.[20]

Nonetheless, while $ZnCl_2$ is low-cost, it is also corrosive at high concentrations. As an alternative approach to reducing H_2O activity, we designed a novel hybrid AZE by using a high concentration of polyethylene glycol 400 (PEG 400) as a crowding agent to form a PEG/H_2O cosolvent. Increased PEG content in 2 m $Zn(OTf)_2$ (≈2.2 M) lowers the conductivity and increases the viscosity as expected (Figure S10). Nonetheless, σ_i is still 0.7 mS cm^{-1} even at 70 wt % PEG (denoted as 70PEG, see Methods), comparable to that of $ZnCl_2$−WiSE.[19] FTIR spectra suggests a strengthened O−H bond owing to the strong H-bonding network between PEG and H_2O (Figure S11), which is anticipated to be less favorable to cleavage at the cathode interface in an electrochemical cell.

We propose that H^+ intercalation at the cathode interface can be effectively suppressed owing to this decreased H_2O activity. Indeed, analysis of the Zn^{2+} solvation structure obtained from MD simulations of the bulk electrolyte shows that the Zn^{2+}−H_2O coordination number in 70PEG (2.3) is lower than in 4 m $Zn(OTf)_2$ (3.3, Figures 4a and S12), reducing the amount of water available to react at the cathode surface. The Zn^{2+}−H_2O coordination distance is similar in all three electrolytes (Figure S13), indicating that the strong Zn^{2+}−H_2O interactions previously observed in $ZnCl_2$ WiSE are operative in 70PEG as well.

Further analysis of our simulations reveals that the fraction of free water is only 16% in 70PEG, compared to 47% in 4 m $Zn(OTf)_2$ and 0% in $ZnCl_2$−WISE (Figure 4c, Table S4), presumably resulting in very low water activity. Examination of the structure of the 70PEG shows that PEG400 molecules aggregate to form PEG-rich regions which absorb water but exclude ions (Figures 4b, d and S14). This finding is consistent with experimental studies, which have shown that PEG aggregates in aqueous solution, forming internally hydrated helical structures that result from the balance of hydrophobic and hydrophilic moieties on the molecule.[21] In 70PEG, this internal hydration reduces the free water content and hinders H_2O molecules from transporting to the cathode interface. Thus, we attribute the reduced H^+ intercalation in $ZnCl_2$−WISE and 70PEG to the low availability and reactivity of water molecules.

Proof of concept was realized by evaluating Zn plating/stripping behavior for the hybrid AZE in Ti‖Zn asymmetric cells, where a very high Coulombic efficiency of around 99.7%
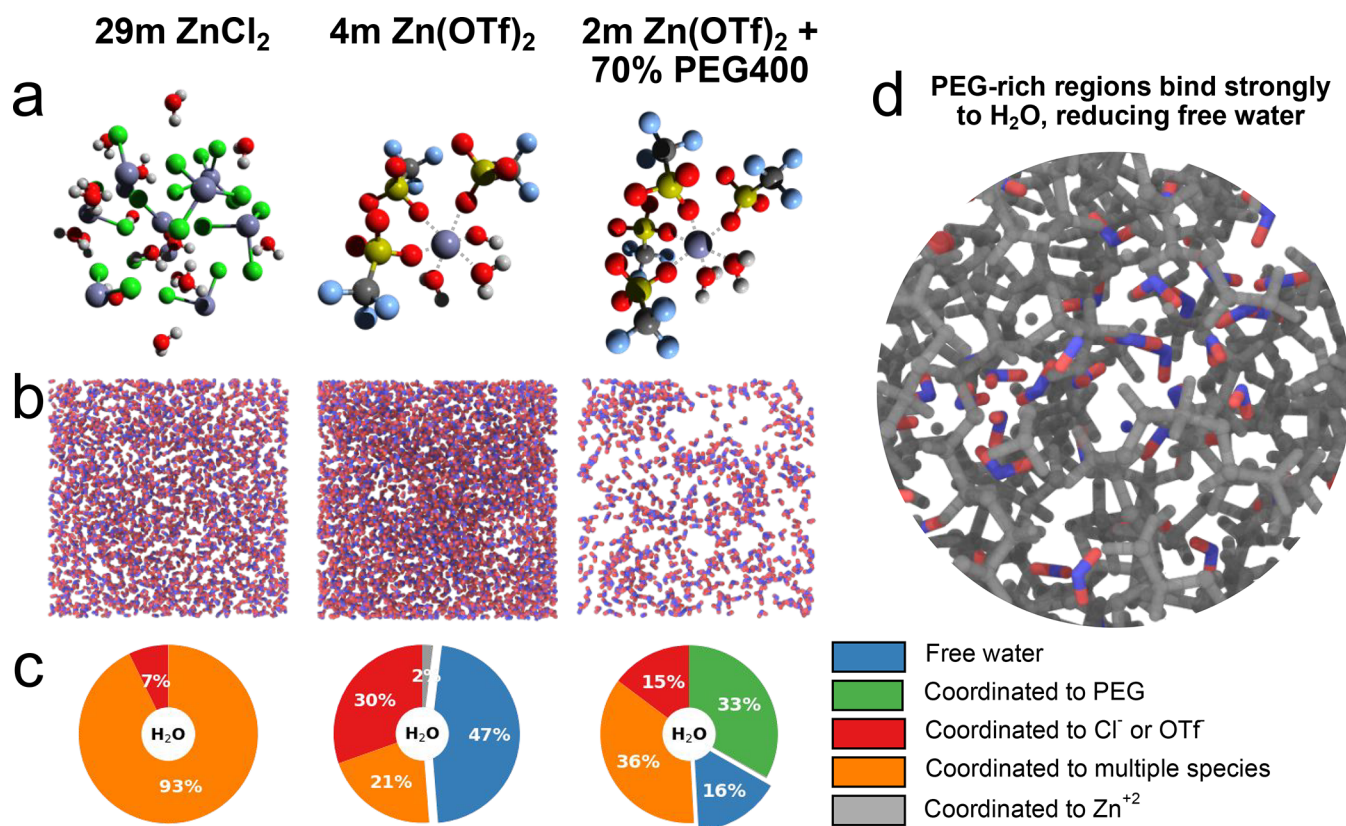
Figure 4. Electrolyte structure in 29 m ZnCl$_2$, 4 m Zn(OTf)$_2$, and 70PEG electrolytes. (a) Typical Zn^{2+} solvation structures. 29 m ZnCl$_2$ WiSE resembles a disordered crystal due to the relative scarcity of water molecules. Zn^{2+} is most commonly coordinated to 3 OTf$^-$ and 3 H$_2$O in 4m Zn(OTf)$_2$, whereas in 70PEG the solvation shell typically comprises 4 OTf$^-$ and 2 H$_2$O. (b) Simulation snapshots showing only the water molecules. (c) Distribution of water populations. (d) Water molecules absorbed into the PEG-rich region of the 70PEG electrolyte.

is achieved for 70PEG at a current density of 1 mA cm^{-2} (1 mAh cm^{-2} capacity), as shown in Figure 5a, b. In contrast, 0PEG cells suffer from extensive dendrite formation under the same operating conditions and failed after three cycles (Figure S15). A Zn∥Zn symmetric cell with 70PEG also functions steadily with a capacity of 1 mAh cm^{-2} over more than 1800 h (>450 cycles), with a denser and more oriented Zn deposition morphology (Figures S16 and S17). Such dendrite-free Zn plating/stripping is consistent with previous work based on a very low weight ratio of PEG or PEO (<1 wt %) in water, where the adsorption of PEG polymer on the electrode surface was proposed to result in more uniform Zn deposition.[22−25] In addition, the electrochemical stability window is expanded to 2.75 V in 70PEG (vs 2.32 V in 0PEG) owing to the reduced water activity (Figure S18).

The 70PEG electrolyte is as efficient for suppressing H$^+$ intercalation as ZnCl$_2$ WiSE in LVP∥Zn full cells (Figure 5c−d). Compared to the second discharge capacity of 115 mAh g^{-1} (∼0.85 Zn^{2+}) in ZnCl$_2$ WiSE, a similar capacity of 112 mAh g^{-1} (∼0.82 Zn^{2+}) is obtained at C/40 in 70PEG (Figure S19). Analysis of the electrode by EDX shows a composition of 0.83 Zn^{2+} per formula unit, suggesting almost all the capacity is contributed by Zn^{2+} intercalation (compared with only 70% in ZnCl$_2$ WiSE). XRD patterns of these two discharged samples are quite similar (Figure 5c); however, the presence of at least three zincated phases lead to a poor Rietveld fit owing to the significant overlap of peaks in these similar structures. Galvanostatic intermittent titration technique (GITT) studies in LVP/70PEG (Figure 5d) yielded an average diffusion

coefficient of ∼10^{-13}−10^{-16} cm^2 s^{-1} that is about 10^2−10^3 lower than previously reported, presumably owing to the lack of significant contribution from H$^+$-ion diffusion.[15] Protons are anticipated to be much more mobile due to their small ionic radius and monovalent property. However, direct comparison with LVP/4 m Zn(OTf)$_2$ could not be obtained due to severe phase transformation resulting from very high degrees of proton intercalation at such a low rate of C/40, where endless discharging was observed (Figure S20). Long-term Zn^{2+} cycling behavior of LVP in PEG was also evaluated at higher rates (Figure 5e). After an initial activation process, LVP can be cycled steadily with a capacity retention of 83.5% after 100 cycles at C/5 and 74.5% after 300 cycles at C/2. Compared to the evolution of the charge/discharge curve profiles upon cycling cells in 4 m Zn(OTf)$_2$, only a slight change can be observed in 70PEG (Figure S21). The absence of a voltage plateau below 0.5 V also indicates the suppression of H$^+$ intercalation.

In summary, our studies of 4 m Zn(OTf)$_2$, 29 m ZnCl$_2$ WiSE, and 2 m Zn(OTf)$_2$ PEG-based hybrid electrolyte on Zn^{2+} versus H$^+$ insertion/extraction of an LVP cathode, reveal the effect of solvation structure and H$_2$O hydrogen bonding network on H$^+$ intercalation. Proton cointercalation verified in 4 m Zn(OTf)$_2$ is suppressed in ZnCl$_2$ WiSE by the interrupted hydrogen bonding network induced by a strong Zn^{2+}−H$_2$O interaction and few free H$_2$O molecules, resulting in dominant Zn^{2+} intercalation that is confirmed quantitatively by Rietveld refinement and EDX. A reduced free water content and further optimized solvation structure was identified in a 2 m Zn(OTf)$_2$
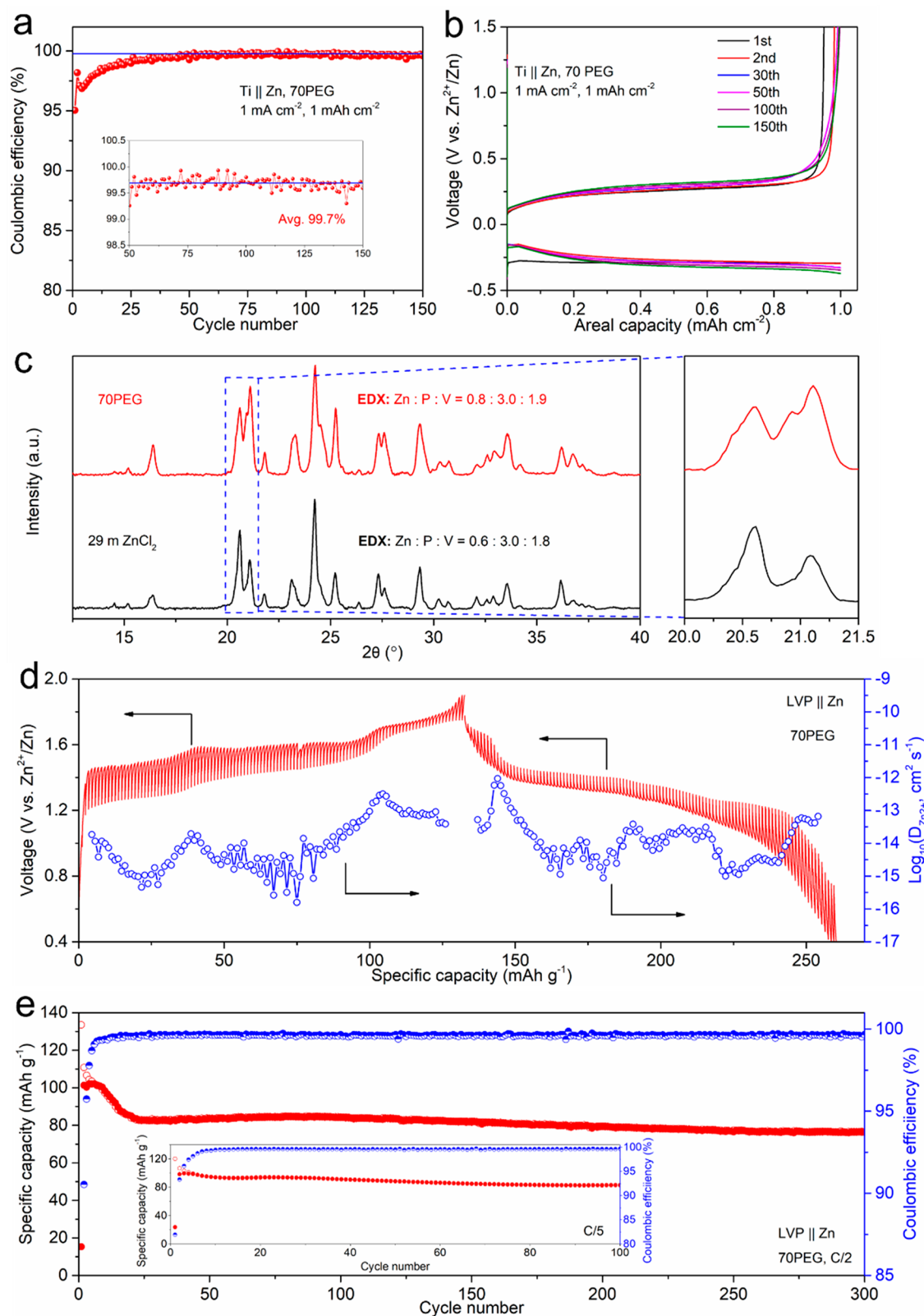
Figure 5. (a) CE evolution over 150 cycles in 70PEG of Ti‖Zn asymmetric cell at 1 mA cm^{-2} for 1 mAh cm^{-2} (Inset = magnified view from 50th to 150th cycles) and (b) corresponding charge−discharge curves. (c) XRD patterns of 2nd fully discharged LVP electrodes in 29 *m* ZnCl$_2$ and 70PEG at C/40 with corresponding EDX ratios of Zn, P and V. (d) GITT profiles and resulting diffusion coefficient data for LVP in 70PEG at C/40; cells were first discharged prior to charge. (e) Capacity retention of LVP in 70PEG at C/2 and C/5 (inset).

PEG-based hybrid electrolyte, where 70PEG shows excellent reversibility and stability for Zn plating/stripping and much better suppression of H$^+$ intercalation due to the strong

interaction between PEG and H$_2$O. The excellent ultra low-rate electrochemical performance (C/40) of LVP in 70PEG also suggests the hybrid electrolyte outperforms the conven-

tional low-concentration aqueous electrolyte to realize dominant Zn^{2+} intercalation. Our work demonstrates that tuning the solvation structure and building strong interactions between H_2O and PEG to interrupt the H_2O hydrogen bonding network is an effective strategy to suppress detrimental H^+ intercalation, maximize Zn^{2+} intercalation, and achieve highly reversible Zn utilization.

■ ASSOCIATED CONTENT

Ⓢ Supporting Information

The Supporting Information is available free of charge at https://pubs.acs.org/doi/10.1021/acsenergylett.1c02514.

> Experimental methods, electrochemical measurements, Rietveld refinements, and lattice parameters (PDF)

■ AUTHOR INFORMATION

Corresponding Author

Linda F. Nazar — *Department of Chemistry and the Waterloo Institute for Nanotechnology, University of Waterloo, Ontario N2L 3G1, Canada; Joint Center of Energy Storage Research, Argonne National Laboratory, Lemont, Illinois 60439, United States;* ⓞ orcid.org/0000-0002-3314-8197; Email: lfnazar@uwaterloo.ca

Authors

Chang Li — *Department of Chemistry and the Waterloo Institute for Nanotechnology, University of Waterloo, Ontario N2L 3G1, Canada; Joint Center of Energy Storage Research, Argonne National Laboratory, Lemont, Illinois 60439, United States*

Ryan Kingsbury — *Energy Storage and Distributed Resources Division, Lawrence Berkeley National Laboratory, Berkeley, California 94720, United States*

Laidong Zhou — *Department of Chemistry and the Waterloo Institute for Nanotechnology, University of Waterloo, Ontario N2L 3G1, Canada; Joint Center of Energy Storage Research, Argonne National Laboratory, Lemont, Illinois 60439, United States;* ⓞ orcid.org/0000-0002-8556-3296

Abhinandan Shyamsunder — *Department of Chemistry and the Waterloo Institute for Nanotechnology, University of Waterloo, Ontario N2L 3G1, Canada; Joint Center of Energy Storage Research, Argonne National Laboratory, Lemont, Illinois 60439, United States*

Kristin A. Persson — *Joint Center of Energy Storage Research, Argonne National Laboratory, Lemont, Illinois 60439, United States; Molecular Foundry, Lawrence Berkeley National Laboratory, Berkeley, California 94720, United States; Department of Materials Science and Engineering, UC Berkeley, Berkeley, California 94720, United States;* ⓞ orcid.org/0000-0003-2495-5509

Complete contact information is available at:
https://pubs.acs.org/10.1021/acsenergylett.1c02514

Author Contributions

C.L. and L.F.N. designed this study. C.L. synthesized the materials, carried out the characterization and all the electrochemical measurements. R.K. and K.A.P. performed molecular dynamics simulations. L.Z. helped with the Rietveld refinements. A.S. helped to perform the GITT measurement. C.L. and L.F.N. wrote the manuscript with contributions from R.K. and K.A.P.

■ REFERENCES

(1) Liu, Z.; Huang, Y.; Huang, Y.; Yang, Q.; Li, X.; Huang, Z.; Zhi, C. Voltage Issue of Aqueous Rechargeable Metal-Ion Batteries. *Chem. Soc. Rev.* **2020**, *49*, 180−232.

(2) Demir-Cakan, R.; Palacin, M. R.; Croguennec, L. Rechargeable Aqueous Electrolyte Batteries: From Univalent to Multivalent Cation Chemistry. *J. Mater. Chem. A* **2019**, *7* (36), 20519−20539.

(3) Blanc, L. E.; Kundu, D.; Nazar, L. F. Scientific Challenges for the Implementation of Zn-Ion Batteries. *Joule* **2020**, *4*, 771−799.

(4) Pan, H.; Shao, Y.; Yan, P.; Cheng, Y.; Han, K. S.; Nie, Z.; Wang, C.; Yang, J.; Li, X.; Bhattacharya, P.; Mueller, K. T.; Liu, J. Reversible Aqueous Zinc/Manganese Oxide Energy Storage from Conversion Reactions. *Nature Energy* **2016**, *1* (5), 16039.

(5) Kundu, D.; Adams, B. D.; Duffort, V.; Vajargah, S. H.; Nazar, L. F. A High-Capacity and Long-Life Aqueous Rechargeable Zinc Battery Using a Metal Oxide Intercalation Cathode. *Nature Energy* **2016**, *1* (10), 16119.

(6) Sun, W.; Wang, F.; Hou, S.; Yang, C.; Fan, X.; Ma, Z.; Gao, T.; Han, F.; Hu, R.; Zhu, M.; Wang, C. Zn/MnO_2 Battery Chemistry With H^+ and Zn^{2+} Coinsertion. *J. Am. Chem. Soc.* **2017**, *139* (29), 9775−9778.

(7) Huang, J.; Wang, Z.; Hou, M.; Dong, X.; Liu, Y.; Wang, Y.; Xia, Y. Polyaniline-Intercalated Manganese Dioxide Nanolayers as a High-Performance Cathode Materials for An Aqueous Zinc-Ion Battery. *Nature Commun.* **2018**, *9*, 2906.

(8) Oberholzer, P.; Tervoort, E.; Bouzid, A.; Pasquarello, A.; Kundu, D. Oxide versus Nonoxide Cathode Materials for Aqueous Zn Batteries: An Insight into the Charge Storage Mechanism and Consequences Thereof. *ACS Appl. Mater. Interfaces* **2019**, *11* (1), 674−682.

(9) Liu, X.; Euchner, H.; Zarrabeitia, M.; Gao, X.; Elia, G. A.; Groß, A.; Passerini, S. Operando pH Measurements Decipher H^+/Zn^{2+} Intercalation Chemsitry in High-Performance Aqueous Zn/β-V_2O_5 Batteries. *ACS Energy Lett.* **2020**, *5*, 2979−2986.

(10) Zhang, L.; Rodriguez-Perez, I. A.; Jiang, H.; Zhang, C.; Leonard, D. P.; Guo, Q.; Wang, W.; Han, S.; Wang, L.; Ji, X. $ZnCl_2$ "Water-in-Salt" Electrolyte Transforms the Performance of Vanadium Oxide as a Zn Battery Cathode. *Adv. Funct. Mater.* **2019**, *29*, 1902653.

(11) Park, M. J.; Yaghoobnejad Asl, H.; Manthiram, A. Multivalent-Ion versus Proton Insertion into Battery Electrodes. *ACS Energy Lett.* **2020**, *5*, 2367−2375.

(12) Ko, J. S.; Paul, P. P.; Wan, G.; Seitzman, N.; DeBlock, R. H.; Dunn, B. S.; Toney, M. F.; Nelson Weker, J. NASCION $Na_3V_2(PO_4)_3$ Enables Quasi-Two-Stage Na^+ and Zn^{2+} Intercalation for Multivalent Zinc Batteries. *Chem. Mater.* **2020**, *32*, 3028−3035.

(13) Shi, H.-Y.; Song, Y.; Qin, Z.; Li, C.; Guo, D.; Liu, X.-X.; Sun, X. Inhibiting $VOPO_4 \cdot xH_2O$ Decomposition and Dissolution in Rechargeable Aqueous Zinc Batteries to Promote Voltage and Capacity Stabilities. *Angew. Chem., Int. Ed.* **2019**, *58* (45), 16057−16061.

(14) Wang, F.; Blanc, L. E.; Li, Q.; Faraone, A.; Ji, X.; Chen-Mayer, H. H.; Paul, R. L.; Dura, J. A.; Hu, E.; Xu, K.; Nazar, L. F.; Wang, C.

Quantifying and Suppressing Proton Intrcalation to Enable High-Voltage Zn-Ion Batteries. *Adv. Energy Mater.* **2021**, *11*, 2102016.

(15) Wang, F.; Hu, E.; Sun, W.; Gao, T.; Ji, X.; Fan, X.; Han, F.; Yang, X.-Q.; Xu, K.; Wang, C. A Rechargeable Aqueous Zn^{2+}-Battery with High Power Density and a Long Cycle-Life. *Energy Environ. Sci.* **2018**, *11* (11), 3168−3175.

(16) Park, M. J.; Yaghoobnejad Asl, H.; Therese, S.; Manthiram, A. Structural Impact of Zn-Insertion into monoclinic $V_2(PO_4)_3$: Implications for Zn-Ion Batteries. *J. Mater. Chem. A* **2019**, *7*, 7159−7167.

(17) Yin, S.; Grondey, H.; Strobel, P.; Anne, M.; Nazar, L. F. Electrochemical Property: Structure Relationships in Monoclinic $Li_{3-y}V_2(PO_4)_3$. *J. Am. Chem. Soc.* **2003**, *125*, 10402−10411.

(18) Yaghoobnejad Asl, H.; Sharma, S.; Manthiram, A. The Critical Effect of Water Content in the Electrolyte on the Reversible Electrochemical Performance of $Zn-VPO_4F$ Cells. *J. Mater. Chem. A* **2020**, *8*, 8262.

(19) Zhang, C.; Holoubek, J.; Wu, X.; Daniyar, A.; Zhu, L.; Chen, C.; Leonard, D. P.; Rodriguez-Perez, I. A.; Jiang, J.; Fang, C.; Ji, X. A $ZnCl_2$ Water-in Salt Electrolyte for A Reversible Zn Metal Anode. *Chem. Commun.* **2018**, *54*, 14097.

(20) Zhang, C.; Shin, W.; Zhu, L.; Chen, C.; Neuefeind, J. C.; Xu, Y.; Allec, S. I.; Liu, C.; Wei, Z.; Daniyar, A.; Jiang, J.-X.; Fang, C.; Alex Greaney, P.; Ji, X. The electrolyte comprising more robust water and superhalides transforms Zn-metal anode reversibly and dendrite-free. *Carbon Energy* **2021**, *3*, 339.
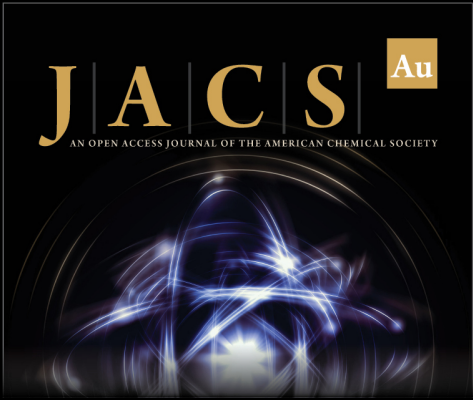
(21) Azri, A.; Giamarchi, P.; Grohens, Y.; Olier, R.; Privat, M. Polyethylene Glycol Aggregates in Water Formed through Hydrophobic Helical Structures. *J. Colloid Interface Sci.* **2012**, *379* (1), 14−19.

(22) Mitha, A.; Yazdi, A. Z.; Ahmed, M.; Chen, P. Surface Adsorption of Polyethylene Glycol to Suppress Dendrite Formation on Zinc Anodes in Rechargeable Aqueous Batteries. *ChemElectroChem.* **2018**, *5*, 2409−2418.

(23) Jin, Y.; Han, K. S.; Shao, Y.; Sushko, M. L.; Xiao, J.; Pan, H.; Liu, J. Stabilizing Zinc Anode Reactions by Polyethelene Oxide Polymer in Mild Aqueous Electrolytes. *Adv. Funct. Mater.* **2020**, *30*, 2003932.

(24) Yan, M.; Xu, C.; Sun, Y.; Pan, H.; Li, H. Manipulating Zn anode reactions through salt anion involving hydrogen bonding network in aqueous electrolytes with PEO additive. *Nano Energy* **2021**, *82*, 105739.

(25) Yan, M.; Dong, N.; Zhao, X.; Sun, Y.; Pan, H. Tailoring the Stability and Kinetics of Zn Anodes through Trace Organic Polymer Additives in Dilute Aqueous Electrolyte. *ACS Energy Lett.* **2021**, *6*, 3236−3243.